Report

Cell Reports

Calcium-Independent Exo-endocytosis Coupling at Small Central Synapses

Graphical Abstract

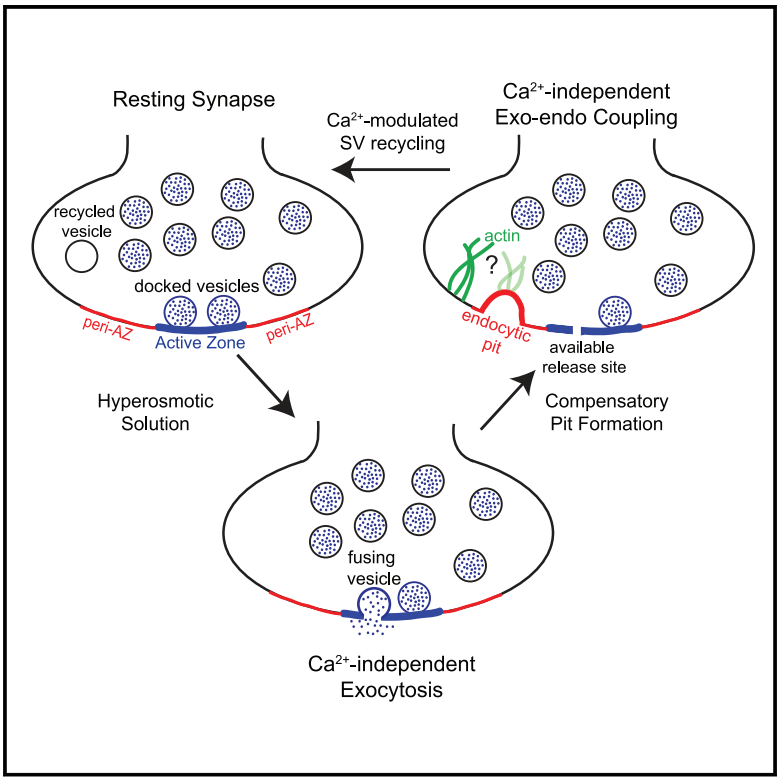

Highlights

- Ca^{2+}-independent synaptic vesicle fusion causes endocytic pit formation
- Sucrose-evoked fusion triggers synaptic vesicle protein and membrane recycling
- Ca^{2+} chelation does not impede endocytic pit formation, but slows endocytosis
- Ca^{2+}-independent endocytic pits require polymerized actin, but not clathrin

Authors

Marta Orlando, Dietmar Schmitz, Christian Rosenmund, Melissa A. Herman

Correspondence

christian.rosenmund@charite.de (C.R.), melissa.herman@charite.de (M.A.H.)

In Brief

As Ca^{2+} is necessary for action-potential-evoked synaptic vesicle fusion, the role of Ca^{2+} in triggering endocytosis is difficult to discern. Orlando et al. find that Ca^{2+}-independent exocytosis triggered by hyperosmotic shock results in the formation of endocytic pits in hippocampal synapses, which depend on actin polymerization.

Orlando et al., 2019, Cell Reports *29*, 3767–3774
December 17, 2019
https://doi.org/10.1016/j.celrep.2019.11.060

CellPress

Cell Reports
Report

Calcium-Independent Exo-endocytosis Coupling at Small Central Synapses

Marta Orlando,[1,6] Dietmar Schmitz,[2,3,4,5] Christian Rosenmund,[1,3,*] and Melissa A. Herman[1,7,*]
[1]Charité-Universitätsmedizin Berlin, corporate member of Freie Universitäts Berlin and Humboldt-Universität zu Berlin, and Berlin Institute of Health, NeuroCure Cluster of Excellence, Institut für Neurophysiologie, Charitéplatz 1, 10117 Berlin, Germany
[2]Charité-Universitätsmedizin Berlin, corporate member of Freie Universitäts Berlin and Humboldt-Universität zu Berlin, and Berlin Institute of Health, NeuroCure Cluster of Excellence, German Center for Neurodegenerative Diseases (DZNE), Charitéplatz 1, 10117 Berlin, Germany
[3]Einstein Center for Neurosciences (ECN), 10117 Berlin, Germany
[4]Bernstein Center for Computational Neuroscience (BCCN) Berlin, 10115 Berlin, Germany
[5]Max-Delbruck-Centrum (MDC) for Molecular Medicine, 13125 Berlin, Germany
[6]Present address: Charité-Universitätsmedizin Berlin, corporate member of Freie Universitäts Berlin and Humboldt-Universität zu Berlin, and Berlin Institute of Health, NeuroCure Cluster of Excellence, Charitéplatz 1, 10117 Berlin, Germany
[7]Lead Contact
*Correspondence: christian.rosenmund@charite.de (C.R.), melissa.herman@charite.de (M.A.H.)
https://doi.org/10.1016/j.celrep.2019.11.060

SUMMARY

At presynaptic terminals, neurotransmitters are released by synaptic vesicle exocytosis at the active zone. In order to maintain efficient neurotransmission and proper synaptic structure, sites of vesicle fusion must be cleared rapidly by endocytosis. Therefore, the coupling of exo- and endocytosis is crucial. Despite many years of research, the exact molecular and biophysical requirements for the coupling of exo- and endocytosis remain unclear. We investigate whether endocytosis can be triggered in a calcium-independent fashion by evoking calcium-independent exocytosis using a hypertonic sucrose solution. We demonstrate that endocytosis can be triggered, in the absence of calcium influx, in a clathrin-independent manner that relies on actin polymerization. Our findings point to a central role of membrane tension dependent on actin for efficient coupling of exo- and endocytosis.

INTRODUCTION

At chemical synapses, a presynaptic electrical signal is converted into a chemical secretory response through the fusion of neurotransmitter-filled synaptic vesicles (SVs) with the plasma membrane. In order to avoid vesicle depletion and to keep synaptic structure constant, SVs need to be reformed after fusion. After spontaneous and evoked SV fusion, membranes and proteins are recycled by endocytosis, a process that retrieves vesicular components from the plasma membrane (Sudhof, 2004). Despite the absolute necessity of endocytosis to sustain neurotransmission and the decades of research into its mechanisms, aspects of the process remain enigmatic (Leitz and Kavalali, 2016; Lou, 2018; Maritzen and Haucke, 2018; Wu et al., 2014a). Pioneering work using membrane capacitance measurements first showed a fast, activity-dependent, and compensatory form of endocytosis for short depolarizing pulses in synaptic terminals (von Gersdorff and Matthews, 1994a, 1994b). In recent years, further insight about the speed of endocytosis has been gained. Based on several studies, it is now evident that endocytosis can occur within tens to hundreds of milliseconds after minimal stimulation at central synapses (Chanaday and Kavalali, 2018a; Delvendahl et al., 2016; Watanabe et al., 2013b)—100 times faster than previously thought (Brockmann and Rosenmund, 2016). The roles for key endocytosis players have also been revised in recent years. Clathrin, a triskelion vesicle coat protein, has long been proposed to be a fundamental component of the retrieval of SV components from the plasma membrane (Royle and Lagnado, 2010; Saheki and De Camilli, 2012); however, recent findings suggest that the reuptake pathway for SV material after evoked fusion is clathrin independent (Soykan et al., 2017; Watanabe et al., 2014; Wu et al., 2014c). Instead, clathrin is proposed to be required for SV reformation from endosomal structures (Kononenko and Haucke, 2015; Watanabe et al., 2014).

The role of Ca^{2+} in SV endocytosis also remains ambiguous (Leitz and Kavalali, 2016; Maritzen and Haucke, 2018). While it is clear that extracellular Ca^{2+} concentration modulates the time course of endocytosis, whether increased Ca^{2+} speeds up (Sankaranarayanan and Ryan, 2001; Zhu et al., 2009) or slows down (Gandhi and Stevens, 2003; Leitz and Kavalali, 2011; von Gersdorff and Matthews, 1994b), the process remains controversial. However, arguably the most difficult aspect to address is the role of Ca^{2+} in exo-endocytosis coupling. While it has been suggested that Ca^{2+} initiates all forms of endocytosis (Wu et al., 2009; Yamashita et al., 2010), addressing the role of Ca^{2+} in triggering endocytosis is a challenge because exocytosis requires Ca^{2+} influx in the presynaptic terminal.

In this study, we asked whether Ca^{2+} is necessary for initiating endocytosis in small central synapses by investigating the synapses' response to Ca^{2+}-independent exocytosis. We addressed this fundamental question by inducing exocytosis with a hypertonic sucrose solution, a well-characterized method to evoke fusion of SVs in a calcium-independent manner (Rosenmund and Stevens, 1996). Using electron microscopy (EM)

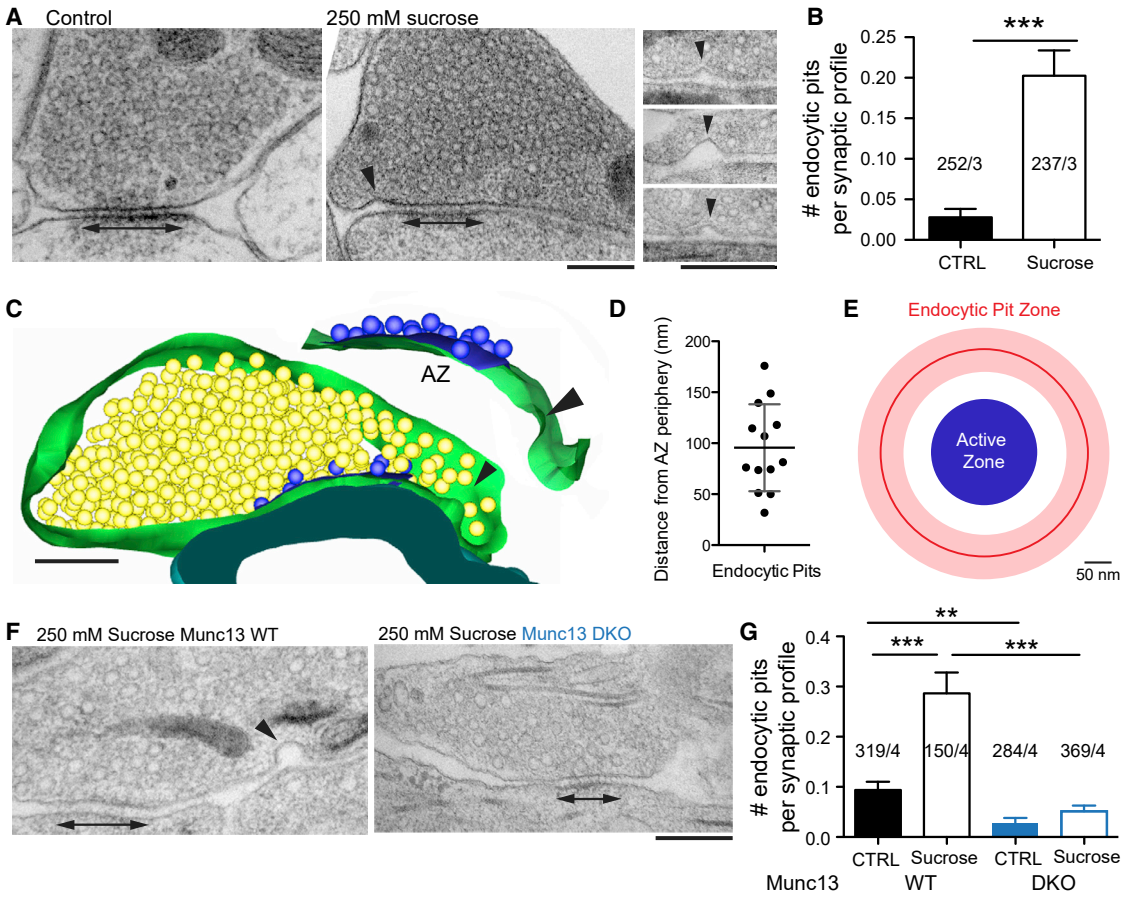

Figure 1. Hypertonic Sucrose-Induced Exocytosis Triggers Membrane Invaginations

(A) Electron micrographs of high-pressure frozen (cryo-fixed) synapses from cultured hippocampal neurons under control conditions or in the presence of 250 mM sucrose (~10 s). Far right shows examples of three membrane invaginations. Black arrows indicate membrane pits.

(B) Membrane invaginations per synaptic profile. Graphs show mean ± SEM. ***$p < 0.0001$.

(C) Serial reconstruction of a cryo-fixed synapse from cultured hippocampal neurons in the presence of 250 mM sucrose hypertonic solution. A membrane invagination (black arrow) occurs ~95 nm from the periphery of the active zone (AZ). Docked SVs and AZ are indicated in blue.

(D and E) Pit distance (peak) from AZ periphery in 13 reconstructed synapses (D) and displayed as simple illustration (E). Black bar in (D) and red circle in (E) are mean ± SD.

(F) Electron micrographs of Munc13 WT and Munc13-1/2 DKO synapses cryo-fixed in the presence of sucrose.

(G) Endocytic pits observed per profile in Munc13 WT or DKO synapses. Graphs show mean ± SEM. **$p = 0.0001$, ***$p < 0.0001$.

For all relevant panels, scale bar is 200 nm. For details of quantification and statistics, please see Table S1. All experiments were performed at room temperature.

analysis of high-pressure frozen cultured hippocampal neurons, we show that Ca^{2+}-independent exocytosis initiates membrane invaginations in presynaptic terminals of small central synapses.

Ca^{2+}-independent exocytosis induced by hypertonic sucrose triggers the formation of endocytic pits at the peri-active zone (peri-AZ) that eventually resolve into SVs. Interestingly, intracellular Ca^{2+} chelation had no effect on the formation of sucrose-induced endocytic pits, but it resulted in a slowing of SV protein recycling. This suggests that while the initial step in exo-endocytosis coupling—the formation of endocytic pits—is completely Ca^{2+} independent, further steps in the endocytosis process are modulated by the presence of Ca^{2+}. Sucrose-induced pits were clathrin independent; however, actin polymerization played a pivotal role in initiating this Ca^{2+}-independent coupling of exo- and endocytosis, likely by maintaining membrane tension in the presynaptic terminal. We propose that the first step in exo-endocytosis coupling is indeed Ca^{2+} independent and is sustained primarily by biophysical properties of the plasma membrane, ensuring the high temporal precision and the exquisite reliability of the process.

RESULTS

Hypertonicity-Induced Exocytosis Triggers Membrane Invaginations

Can exo-endocytosis coupling occur in a Ca^{2+}-independent manner? To answer this question, we examined the ultrastructure of synapses from cultured hippocampal neurons exposed to a hypertonic sucrose solution (Figure 1). A hypertonic sucrose solution has been shown, by physiological methods, to cause

the release of neurotransmitters in a calcium-independent manner (Rosenmund and Stevens, 1996). In high-pressure frozen, or cryo-fixed, samples processed for transmission EM analysis, we found membrane invaginations formed in synapses frozen during exposure to hypertonic sucrose solutions, occurring in the periphery of the AZ (Figures 1A and 1B; ~10 s of 250 mM sucrose). Additionally, we found that the density of SVs within a synaptic terminal increased with sucrose application, likely because of shrinkage caused by the hypertonic solution (control: 187.9 ± 8.93 SVs/μm^2; sucrose: 232 ± 6.553 SVs/μm^2; ****$p < 0.0001$; Mann-Whitney test; mean ± SEM). Analysis of 13 three-dimensionally reconstructed synapses showed that invaginations occurred within 96 ± 12 nm of the AZ, consistent with occurrence of membrane invaginations in the peri- AZ region (Lou, 2018; Figures 1C–1E). These data strongly suggest the identity of sucrose-induced membrane invaginations as endocytic pits.

To confirm that the sucrose-induced invaginations are a consequence of exocytosis, we performed similar experiments in Munc13-1/2 double knockout (Munc13 DKO) neurons, which are incapable of SV fusion (Augustin et al., 1999; Varoqueaux et al., 2002). Indeed, we did not observe increased numbers of endocytic pits in Munc13 DKO synapses frozen in the presence of sucrose, while a clear increase was observed in the Munc13-1 wild-type/Munc13-2 knockout (Munc13 WT) littermate synapses (Figures 1F and 1G). Interestingly, more pits were also observed in Munc13 WT than in DKO littermate synapses during control conditions (Figures 1F and 1G), suggesting that similar structures are induced by spontaneous release of SVs, which is absent in Munc13 DKO synapses (Varoqueaux et al., 2002).

Previous work strongly suggests that hypertonic sucrose-evoked neurotransmitter release is calcium independent (Rosenmund and Stevens, 1996). However, to further confirm these results, we performed live-cell imaging in cultured neurons expressing the synapse-localized, genetically encoded Ca^{2+} sensor, SynGCaMP6f (Figure S1A; Grauel et al., 2016). SynGCaMP6f showed a robust response to a field stimulation of 10 or 40 stimuli at 20 Hz (Figures S1B–S1D). A clear increase in SynGCaMP6f fluorescence was also detectable in response to a single stimulus, albeit significantly smaller than the train stimuli (Figures S1B–S1E). However, a peak SynGCaMP6f fluorescence response was nearly undetectable during a 10-s application of 250 mM hypertonic sucrose solution (Figures S1B and S1E). The SynGCaMP6f response to 250 mM hypertonic solution (10 s) was also unchanged in the presence of low $[Ca^{2+}]_e$ (0.1 mM) or tetrodotoxin (TTX; 1 μM; Figure S1E), while, as expected, the 10 or 40 stimuli trains were nearly abolished in low $[Ca^{2+}]_e$ or TTX (Figures S1C and S1D).

Calcium-Independent Exocytosis Triggers Endocytosis, SV Protein Retrieval, and SV Reformation

Previous work suggests that hypertonic sucrose can stimulate the endocytosis process (Pyle et al., 2000). However, to confirm that Ca^{2+}-independent exocytosis in our hands triggers the full process of endocytosis, not only endocytic pit formation, we first investigated SV protein recycling using live-cell imaging of the pH-sensitive variant of GFP and the SV cycle reporter, SypHy (Figure 2). For SypHy experiments, sucrose was pulsed onto cultured neurons using a fast-flow perfusion system during imaging. To ensure both a rapid and robust hypertonic-solution-evoked release, we chose a concentration of 500 mM sucrose applied for 2 s, though a 250-mM sucrose application for 10 s also produced a detectable change in fluorescence (Figure S2A). The decay time constant for the 250-mM sucrose SypHy signal was significantly faster than that for 500-mM sucrose (6.3 ± 0.4 s and 7.8 ± 0.4 s, respectively; *$p = 0.0107$, unpaired t test). Because of the robust response to a briefer pulse, we used 500 mM sucrose for the subsequent SypHy experiments. We found that the average peak SypHy signal (normalized to the 50-mM NH_4Cl response) evoked by a 500-mM sucrose application was smaller than a 40-pulse stimulus train at 20 Hz, but indistinguishable from 20 stimuli at 10 Hz under control conditions (Figures 2A and 2B). Like the Ca^{2+}-evoked signals, the sucrose-evoked SypHy signal had a peak followed by a decay of the fluorescence, indicative of the retrieval and reacidification of SV proteins. To investigate the kinetics of the SV recycling process of Ca^{2+}-dependent or Ca^{2+}-independent exocytosis, we measured the width of the SypHy signal at 50% of the peak. With this measure, we found no difference between the sucrose-evoked response and the train stimulations (Figure 2C). Finally, we compared the SypHy-signal-evoked sucrose in control conditions to that in the presence of low $[Ca^{2+}]_e$ or TTX and found no effect on either the peak SypHy signal or the width at 50% of the peak with either treatment (Figures S2B–S2D), again confirming that the sucrose-evoked exocytosis is occurring in the absence of Ca^{2+} influx.

Does sucrose-evoked endocytosis rely on critical molecular players typically involved in SV retrieval at the plasma membrane, such as dyanmin (Koenig and Ikeda, 1989; Ferguson et al., 2007)? To examine this, we measured the sucrose-evoked SypHy response before and after acute inhibition of dynamin with dynasore (80 μM, 3 min; Figures 2D and 2E). We found that while dynasore had a small, but significant, effect on the peak of the sucrose-evoked fluorescence (83% ± 5% of control; *$p = 0.0293$; paired t test; Figure 2D), the amount by which the signal had decayed in 30 s following the sucrose application was dramatically reduced (Figures 2D and 2E). These data show that, indeed, sucrose-evoked endocytosis requires dynamin.

To investigate whether membrane structures are also recycled after Ca^{2+}-independent exocytosis, we incubated neurons in an extracellular solution containing the soluble marker, ferritin, prior to cryo-fixation in sucrose, or at different time points after sucrose washout (i.e., ~10 and 30 s, respectively; Figure 2F). With EM, we observed that ferritin was internalized into SVs in a graded manner between 10 and 30 s after sucrose-induced exocytosis (Figures 2F and 2G), indicating that endocytosis as well as SV reformation can be triggered in a Ca^{2+}-independent fashion at small central synapses. Interestingly, we found no ferritin-positive SVs in synapses cryo-fixed in the presence of sucrose, which lasts approximately 10 s (Figures 2F and 2G). This suggests that sucrose itself inhibits the progression of endocytosis past the point of pit formation, allowing us to preserve the membrane invaginations for ultrastructural analysis, while endocytosis proceeds only upon sucrose washout (see also Figure S2A).

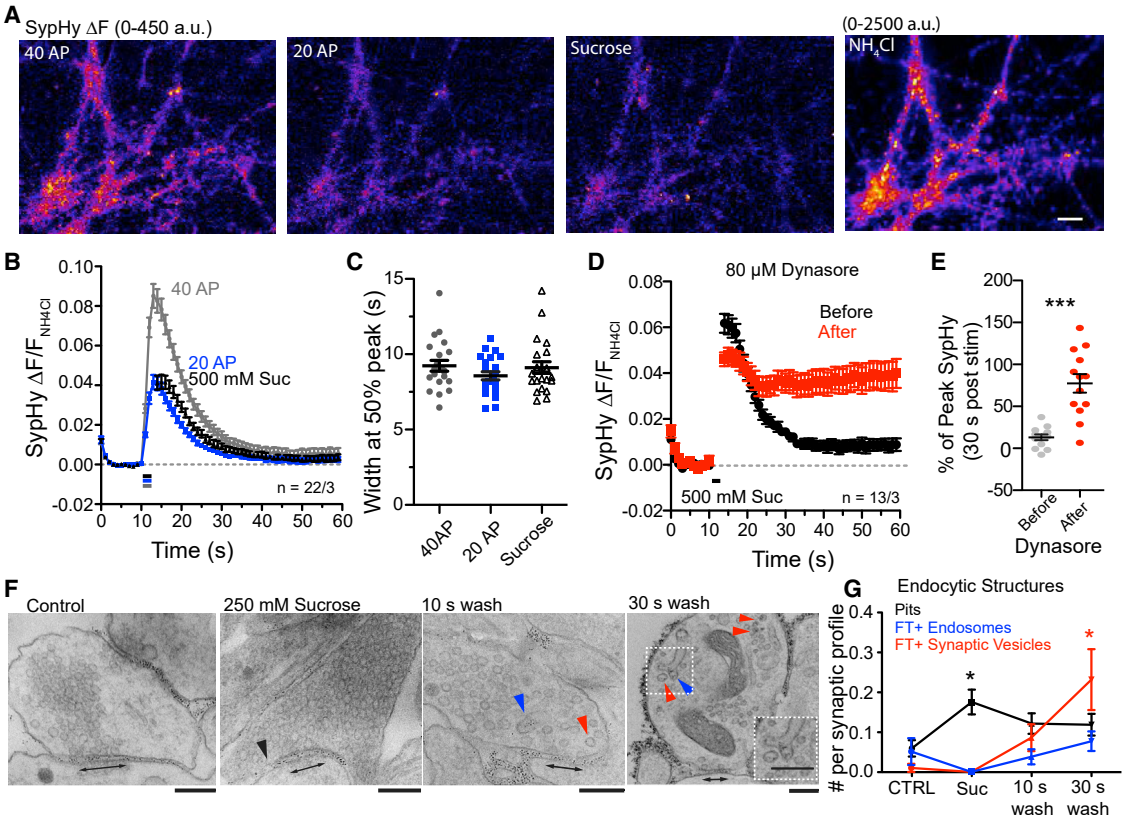

Figure 2. Sucrose Triggers Endocytosis and SV Reformation

(A) Images of cultures expressing SypHy stimulated with 40 pulses inducing action potentials (APs) at 20 Hz, 20 pulses at 10 Hz, or 500 mM sucrose for 2 s. 50 mM ammonium chloride (NH_4Cl: far right panel) is used to identify areas of interest and normalize stimulated SypHy signals. Scale bar, 10 μm. All SypHy experiments were performed at ~32°C-34°C.

(B) Average ammonium-normalized SypHy signal in response to indicated stimulation protocols over time. For illustrative purposes, SypHy values during the sucrose application have been blanked.

(C) Average width of SypHy signals at 50% of the peak measured per image in response to indicated stimulation protocols.

(D) Average ammonium-normalized SypHy signal evoked by application of 500 mM sucrose over time before and after application of 80 μM dynasore (3 min).

(E) SypHy response normalized to peak at 30 s post-sucrose pulse before and after treatment with 80 μM dynasore. ***$p < 0.0001$.

(F) Electron micrographs of high-pressure frozen cultured hippocampal synapses cryo-fixed, after ferritin incubation, either in control conditions or in 250 mM sucrose (~10 s), or 10 s or 30 s, respectively, after sucrose treatment (wash). Scale bars, 200 nm. Experiments were performed at 35°C.

(G) Quantification of endocytic pits (black), ferritin-positive endosomes (blue), or ferritin-positive SVs (red) occurring in each condition. *$p \leq 0.05$.

Color of arrows in (E) indicate presence of structure described in (F). All experiments in (G) were performed in the presence of TTX (1 μM). The n values in (F) are from 98–164 synaptic profiles. Graphs in all panels show mean ± SEM. For details of quantification and statistics, please see Table S1.

Intracellular Calcium Buffering Affects Endocytosis Kinetics but Not Pit Formation

We next investigated whether not only Ca^{2+} influx, but also intracellular Ca^{2+}, affects sucrose-induced endocytosis (Figure 3). We incubated cultures in BAPTA-AM for 5–10 min (20 μM at 37°C). Analysis of high-pressure frozen samples by EM revealed no change in endocytic pits induced by sucrose in BAPTA-treated synapses compared to control (Figures 3A and 3B). However, the peak SypHy signal evoked by a 500-mM sucrose pulse was equally reduced with BAPTA incubation of 5 or 10 min (69% ± 5% or 59% ± 5%, respectively; mean ± SEM; Figure 3C), and, interestingly, the width of the signal at 50% of the peak was increased in a graded manner with 5 or 10 min incubation (127% ± 6% or 150% ± 7% of control, respectively; mean ± SEM; Figure 3D). In addition to the width of the signal, the decay time course was also increased by incubation with BAPTA-AM (τ = 8.0 ± 0.5 s, DMSO; 12.8 ± 1.1 s, 5 min BAPTA; 13.7 ± 0.9 s, 10 min BAPTA; mean ± SEM). Taken together, these results suggest that while the initial coupling of exo-endocytosis is Ca^{2+} independent, the resolution of endocytic pits is modulated by Ca^{2+}, potentially even basal intracellular Ca^{2+}, consistent with previous work showing intracellular Ca^{2+} chelation or elimination of Ca^{2+}-binding proteins slowing down basal endocytosis rates (Miyano et al., 2019; Wu et al., 2009, 2014b).

Calcium-Independent Exo-endocytosis Coupling Requires Actin Polymerization but Not Clathrin

What are the molecular and biophysical requirements of the initial step in Ca^{2+}-independent exo-endocytosis coupling, the formation of endocytic pits? As elevated temperature is a requirement

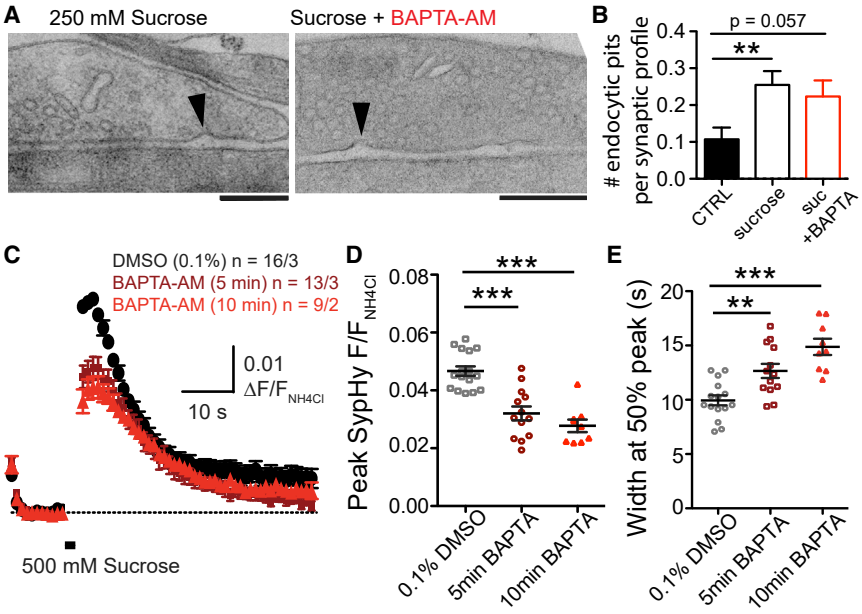

Figure 3. Intracellular Ca^{2+} Buffering Affects Endocytosis Kinetics but not Pit Formation

(A) Electron micrographs of high-pressure frozen synapses, cryo-fixed in the presence of 250 mM sucrose with or without pre-incubation in BAPTA-AM (20 μM, 10 min at 37°C). Scale bars, 200 nm. Experiments were performed at 35°C.

(B) Average number of endocytic pits per synaptic profile. Control, n = 112/2; sucrose, n = 149/2; sucrose+BAPTA-AM, n = 103/2. **p = 0.0061.

(C) Average ammonium chloride-normalized SypHy signal over time in response to 500 mM sucrose (2 s) in control conditions (0.1% DMSO, 5-10 min, 37°C; black) or after pre-incubation with BAPTA-AM (20 μM at 37°C) for 5 min (dark red) or 10 min (red). SypHy imaging was performed at ~32°C-34°C.

(D and E) Comparison of the SypHy response peaks (D) or widths at 50% peak (E) in indicated conditions. **p ≤ 0.01, ***p ≤ 0.001.

For details of quantification and statistics, please see Table S1.

for the initiation of ultrafast endocytosis under mild stimulation conditions (Delvendahl et al., 2016; Watanabe et al., 2013b), we tested whether sucrose induction of endocytic pits is also temperature dependent. Interestingly, we found no difference in the average number of endocytic pits formed in the presence of -sucrose in synapses cryo-fixed at 25°C or 35°C (Figures 4A and 4B). This suggests, under our stimulation conditions, that Ca^{2+}-independent exocytosis can drive endocytic pit formation. It should be noted that there is no temporal resolution with the sucrose application; thus, we have no information about the temperature-dependent kinetics of pit formation. As endocytosis shows a clear temperature dependence (Delvendahl et al., 2016; Renden and von Gersdorff, 2007), it is likely that this form of endocytosis is also slower at room temperature than at near-physiological temperature.

What molecular machinery is responsible for pit formation? We investigated whether clathrin, the coat protein classically thought to drive endocytosis from the plasma membrane (Heuser and Reese, 1973; Milosevic, 2018), is involved in the initiation of sucrose-evoked endocytic pits. EM analysis of cryo-fixed synapses revealed that sucrose evoked endocytic pits in synapses expressing shRNA against clathrin heavy chain (CKD; (Kononenko et al., 2014; Soykan et al., 2017; Watanabe et al., 2014) to the same extent as those expressing a scramble (Scr) shRNA (Figures 4C and 4D). This result is in line with previous work suggesting that the main role of clathrin in the SV cycle is to reform SVs from endosomal intermediates and not from the plasma membrane (Kononenko et al., 2014; Milosevic, 2018; Soykan et al., 2017; Watanabe et al., 2014).

Formation of sucrose-evoked, Ca^{2+}-independent endocytic pits requires membrane insertion (Figures 1F and 1G) but is clathrin independent (Figures 4C and 4D). As actin is proposed to play a pivotal role in clathrin-independent endocytosis (Soykan et al., 2017; Watanabe et al., 2013b), we tested whether Ca^{2+}-independent endocytic pit formation was affected by inhibiting actin polymerization. We found that treating cultures with the actin polymerization inhibitor, latrunculin-A (10 μM), significantly impeded the formation of endocytic pits in sucrose (Figures 4E and 4F). This suggests a critical role for actin polymerization in the formation of the endocytic pit.

Remarkably, while latrunculin-A treatment strongly impeded sucrose-induced pit formation, consistent with its inhibition of endocytic pit formation after mild stimulation in ultrafast endocytosis (Watanabe et al., 2013b), neither latrunculin-A treatment (5 μM) nor clathrin shRNA affected the time course of SV protein retrieval after sucrose stimulation, as assayed by SypHy (Figures S3A, S3C, and S3D). Clathrin shRNA did, however, increase the fraction of total SypHy residing on the surface, suggesting that the clathrin knockdown was effective and indeed had a physiological effect in the neurons (Figure S3B). The lack of change in SypHy time course with either treatment (Figure S3) suggests that multiple recycling pathways are active in parallel. Whether SV proteins are recycled through different endocytic structures when the clathrin-independent mode of endocytosis is impaired will be a subject of future investigations.

DISCUSSION

In this work, we show that endocytosis is coupled to exocytosis in a Ca^{2+}-independent manner and that Ca^{2+} rather plays a role in modulating the subsequent steps of the endocytosis process. We suggest that the triggering of endocytosis is mediated by biophysical changes induced by the addition of an SV membrane to the plasma membrane and that actin-mediated membrane tension plays a crucial role in this process. By inducing Ca^{2+}-independent exocytosis, we reveal that this fundamental, compensatory membrane retrieval process is indeed initiated in a Ca^{2+}-independent manner.

What is the evidence that the sucrose-induced structures are not fusion events? First, we point to the location of the pits

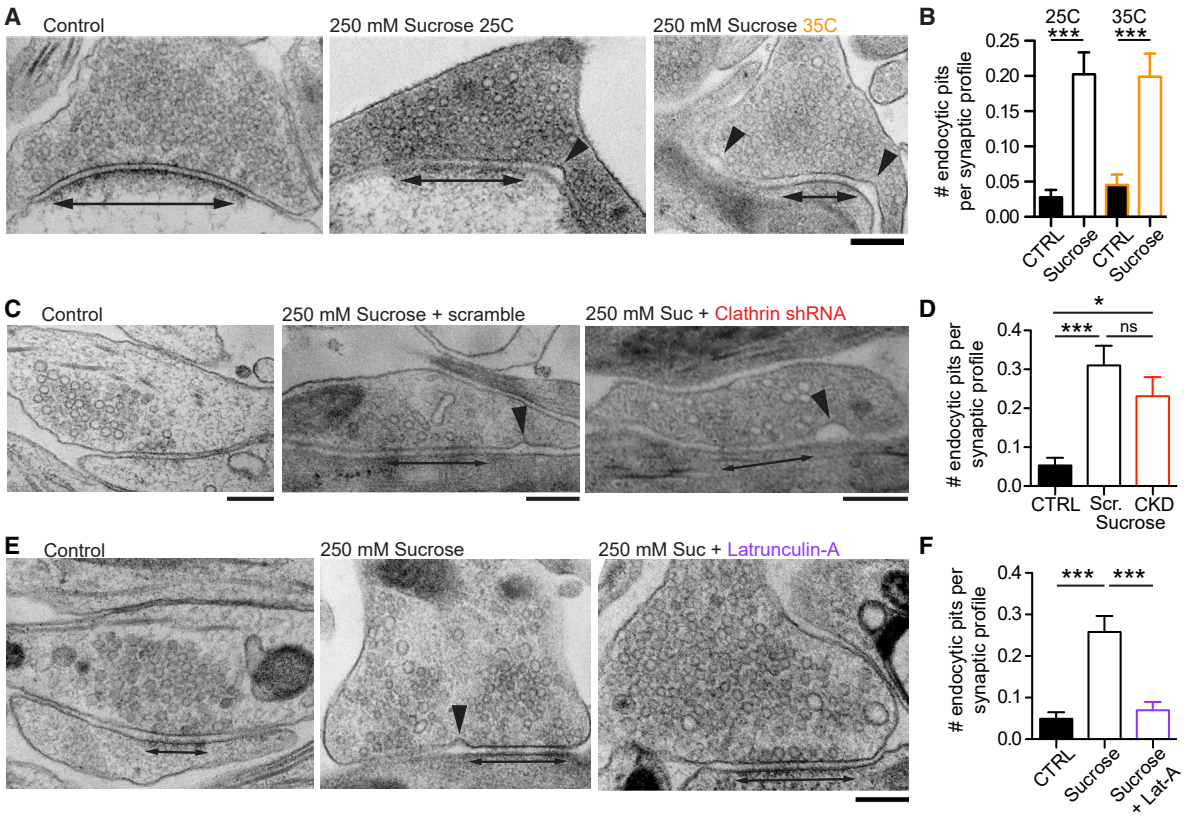

Figure 4. Ca^{2+}-Independent Endocytic Pits Depend on Actin Polymerization, but not Clathrin

(A) Electron micrographs of hippocampal synapses cryo-fixed in control extracellular solution or in the presence of 250 mM sucrose (~10 s) at 25°C or 35°C.

(B) Endocytic pits per synaptic profile in 250 mM sucrose at 25°C or 35°C and temperature-matched control. Control 25°C, n = 252/3; sucrose 25°C, n = 237/3; control 35°C, n = 198/5; sucrose 35°C, n = 216/5. ***p ≤ 0.002.

(C) Electron micrographs of a synapse expressing a scramble shRNA (Scr.) cryo-fixed in control extracellular solution or synapses expressing either scramble shRNA or shRNA against the clathrin heavy chain (CKD) cryo-fixed in the presence of 250 mM sucrose (~10 s).

(D) Endocytic pits observed per synaptic profile in conditions described in (C). Control Scr., n = 131/2; sucrose Scr., n = 100/2; sucrose CKD, n = 108/2. Experiments were performed at room temperature. *p = 0.0218, ***p ≤ 0.0001.

(E) Electron micrographs of hippocampal synapses cryo-fixed in control extracellular (0.01% DMSO), 250 mM sucrose (0.01% DMSO), or 250 mM sucrose + latrunculin-A (10 μM). Experiments were performed at 35°C.

(F) Endocytic pits observed per synaptic profile in conditions described in (E). Control, n = 184/3; sucrose, n = 151/3; sucrose+LAT-A, n = 158/3. ***p ≤ 0.0003. Scale bars for all relevant panels, 200 nm. All data are presented as mean ± SEM. For details of quantification and statistics, please see Table S1.

peripheral to the AZ structure (Figure 1). The three-dimensional (3D) reconstruction of synapses in particular provides excellent spatial resolution for the sucrose-induced pits, which always occur in regions outside of the AZ. Second, the inhibition of actin polymerization by latrunculin-A completely abolishes sucrose-induced pits (Figures 4E and 4F) but has no effect on the peak sucrose-evoked SypHy signal, which reflects no change in exocytosis (Figure S3B). Taken together, these results provide convincing evidence that the sucrose-induced structures are endocytic pits.

Morphologically and mechanistically, our sucrose-induced endocytic pits are reminiscent of those initiating ultrafast endocytosis (Watanabe et al., 2013b, 2014). However, while we show no temperature dependence on the occurrence of sucrose-induced structures (Figures 4A and 4B), the sucrose method lacks temporal resolution and, thus, does not provide information about the speed at which endocytic pits form at room temperature. Nevertheless, endocytic pits after mild stimulation occur at an elevated temperature but are impeded at room temperature (Watanabe et al., 2013b). We argue that this apparent discrepancy arises from the higher membrane load added to presynaptic terminals with sucrose stimulation versus a single action potential (AP) (Arancillo et al., 2013). Because the fluidity of the membrane is temperature dependent (Chanaday and Kavalali, 2018b), it may take more added SV membrane to result in the membrane invagination at 25°C (more rigid membrane) than at 35°C (more fluid membrane). In support of this hypothesis, ultrafast endocytic pits were also observed in *C. elegans* neuromuscular junction with a single AP at room temperature (Watanabe et al., 2013a). Therefore, temperature may serve as the gateway to the clathrin-independent ultrafast endocytosis pathway at small central synapses by influencing the biophysical properties of the membrane.

Actin's precise role in endocytic pit formation is still enigmatic. We suggest two potential modes: (1) an area of increased tension in the peri-AZ region generated by actin polymerization or (2) active pulling of the membrane by actin at the peak of the pits in response to the added membrane. Differentiation between the two will require both localization of actin within the peri-AZ region and further analysis of molecular partners, such as formin (Soykan et al., 2017). Downstream molecular mechanisms most likely include sensing of the membrane curvature by BAR proteins, such as endophilin, which is important for the neck formation of endocytic pits (Watanabe et al., 2018).

Unmasking of the Ca^{2+}-independent properties of exo-endocytosis coupling at small central synapses emphasizes the importance of SV membrane clearance and homeostasis of plasma membrane tension and structure. This discovery opens the door to many exciting questions. For instance, how is the membrane fluidity compartmentalized to the peri-AZ region? Do similar Ca^{2+}-independent endocytic membrane structures occur at synapses with many more AZs, such as the mossy fiber bouton, where the speed and initiation of endocytosis has also recently been shown to be Ca^{2+} independent (Miyano et al., 2019; Wu et al., 2009; Yamashita et al., 2010)? Are the same molecular players involved in the resolution of Ca^{2+}-independent, sucrose-induced endocytic pits as those required for ultrafast endocytosis (Watanabe et al., 2018)? Finally, what is the mechanism that senses membrane invaginations in the peri-AZ to initiate their resolution? We believe that our findings provide a springboard for future work addressing these issues and can help pave the way toward a better understanding of the crucial and fundamental process of exo-endocytosis coupling at chemical synapses.

STAR★METHODS

Detailed methods are provided in the online version of this paper and include the following:

- KEY RESOURCES TABLE
- LEAD CONTACT AND MATERIALS AVAILABILITY
- EXPERIMENTAL MODEL AND SUBJECT DETAILS
- METHOD DETAILS
  - Cloning and molecular biology
  - Live imaging of SypHy and SynGCaMP6f
  - Electron microscopy
- QUANTIFICATION AND STATISTICAL ANALYSIS
  - Live imaging of SypHy and SynGCaMP6f
  - Electron microscopy
- DATA AND CODE AVAILABILITY

SUPPLEMENTAL INFORMATION

Supplemental Information can be found online at https://doi.org/10.1016/j.celrep.2019.11.060.

ACKNOWLEDGMENTS

We thank the Charité Viral Core Facility for molecular tools, B. Söhl-Kielczynski for expert technical support, S.H. Hosseini for image analysis, Dr. M. Camacho-Perez for Munc13DKO cultures, the Statistik-Ambulanz (Institut für Biometrie und Klinische Epidemiologie, Charité-Universitätsmedizin) for statistics consultation, and Prof. Dr. C. Garner and the Rosenmund lab for discussions. This work was funded by the Deutsche Forschungsgemeinschaft (DFG, German Research Council) - Project # 319489780 - HE7480/2-1 (to M.A.H.); Horizon 2020 ERA-NET Neuron - Grant ID ADIKHUMICE (to C.R.); and Deutsche Forschungsgemeinschaft (DFG, German Research Foundation) under Germany's Excellence Strategy – EXC-2049 – 390688087 (to D.S. and C.R.).

AUTHOR CONTRIBUTIONS

Conceptualization, Methodology, Formal Analysis, Investigation, and Writing, M.O. and M.A.H.; Validation and Supervision, C.R.; Funding Acquisition, M.A.H., D.S., and C.R.

DECLARATION OF INTERESTS

The authors declare no competing interests.

Received: August 26, 2019
Revised: October 8, 2019
Accepted: November 14, 2019
Published: December 17, 2019

REFERENCES

Arancillo, M., Min, S.W., Gerber, S., Münster-Wandowski, A., Wu, Y.J., Herman, M., Trimbuch, T., Rah, J.C., Ahnert-Hilger, G., Riedel, D., et al. (2013). Titration of Syntaxin1 in mammalian synapses reveals multiple roles in vesicle docking, priming, and release probability. J. Neurosci. *33*, 16698–16714.

Augustin, I., Rosenmund, C., Südhof, T.C., and Brose, N. (1999). Munc13-1 is essential for fusion competence of glutamatergic synaptic vesicles. Nature *400*, 457–461.

Brockmann, M.M., and Rosenmund, C. (2016). Catching Up with Ultrafast Endocytosis. Neuron *90*, 423–424.

Camacho, M., Basu, J., Trimbuch, T., Chang, S., Pulido-Lozano, C., Chang, S.S., Duluvova, I., Abo-Rady, M., Rizo, J., and Rosenmund, C. (2017). Heterodimerization of Munc13 C_2A domain with RIM regulates synaptic vesicle docking and priming. Nat. Commun. *8*, 15293.

Chanaday, N.L., and Kavalali, E.T. (2018a). Optical detection of three modes of endocytosis at hippocampal synapses. eLife *7*, e36097.

Chanaday, N.L., and Kavalali, E.T. (2018b). Time course and temperature dependence of synaptic vesicle endocytosis. FEBS Lett. *592*, 3606–3614.

Chen, T.W., Wardill, T.J., Sun, Y., Pulver, S.R., Renninger, S.L., Baohan, A., Schreiter, E.R., Kerr, R.A., Orger, M.B., Jayaraman, V., et al. (2013). Ultrasensitive fluorescent proteins for imaging neuronal activity. Nature *499*, 295–300.

Delvendahl, I., Vyleta, N.P., von Gersdorff, H., and Hallermann, S. (2016). Fast, Temperature-Sensitive and Clathrin-Independent Endocytosis at Central Synapses. Neuron *90*, 492–498.

Ferguson, S.M., Brasnjo, G., Hayashi, M., Wölfel, M., Collesi, C., Giovedi, S., Raimondi, A., Gong, L.W., Ariel, P., Paradise, S., et al. (2007). A selective activity-dependent requirement for dynamin 1 in synaptic vesicle endocytosis. Science *316*, 570–574.

Gandhi, S.P., and Stevens, C.F. (2003). Three modes of synaptic vesicular recycling revealed by single-vesicle imaging. Nature *423*, 607–613.

Grauel, M.K., Maglione, M., Reddy-Alla, S., Willmes, C.G., Brockmann, M.M., Trimbuch, T., Rosenmund, T., Pangalos, M., Vardar, G., Stumpf, A., et al. (2016). RIM-binding protein 2 regulates release probability by fine-tuning calcium channel localization at murine hippocampal synapses. Proc. Natl. Acad. Sci. USA *113*, 11615–11620.

Herman, M.A., Trimbuch, T., and Rosenmund, C. (2018). Differential pH Dynamics in Synaptic Vesicles From Intact Glutamatergic and GABAergic Synapses. Front. Synaptic Neurosci. *10*, 44.

Heuser, J.E., and Reese, T.S. (1973). Evidence for recycling of synaptic vesicle membrane during transmitter release at the frog neuromuscular junction. J. Cell Biol. *57*, 315–344.

Koenig, J.H., and Ikeda, K. (1989). Disappearance and reformation of synaptic vesicle membrane upon transmitter release observed under reversible blockage of membrane retrieval. J. Neurosci. *9*, 3844–3860.

Kononenko, N.L., and Haucke, V. (2015). Molecular mechanisms of presynaptic membrane retrieval and synaptic vesicle reformation. Neuron *85*, 484–496.

Kononenko, N.L., Puchkov, D., Classen, G.A., Walter, A.M., Pechstein, A., Sawade, L., Kaempf, N., Trimbuch, T., Lorenz, D., Rosenmund, C., et al. (2014). Clathrin/AP-2 mediate synaptic vesicle reformation from endosome-like vacuoles but are not essential for membrane retrieval at central synapses. Neuron *82*, 981–988.

Leitz, J., and Kavalali, E.T. (2011). Ca^{2+} influx slows single synaptic vesicle endocytosis. J. Neurosci. *31*, 16318–16326.

Leitz, J., and Kavalali, E.T. (2016). Ca2+ Dependence of Synaptic Vesicle Endocytosis. Neuroscientist *22*, 464–476.

Lois, C., Hong, E.J., Pease, S., Brown, E.J., and Baltimore, D. (2002). Germline transmission and tissue-specific expression of transgenes delivered by lentiviral vectors. Science *295*, 868–872.

Lou, X. (2018). Sensing Exocytosis and Triggering Endocytosis at Synapses: Synaptic Vesicle Exocytosis-Endocytosis Coupling. Front. Cell. Neurosci. *12*, 66.

Maritzen, T., and Haucke, V. (2018). Coupling of exocytosis and endocytosis at the presynaptic active zone. Neurosci. Res. *127*, 45–52.

Milosevic, I. (2018). Revisiting the Role of Clathrin-Mediated Endoytosis in Synaptic Vesicle Recycling. Front. Cell. Neurosci. *12*, 27.

Miyano, R., Miki, T., and Sakaba, T. (2019). Ca-dependence of synaptic vesicle exocytosis and endocytosis at the hippocampal mossy fibre terminal. J. Physiol. *597*, 4373–4386.

Pyle, J.L., Kavalali, E.T., Piedras-Rentería, E.S., and Tsien, R.W. (2000). Rapid reuse of readily releasable pool vesicles at hippocampal synapses. Neuron *28*, 221–231.

Renden, R., and von Gersdorff, H. (2007). Synaptic vesicle endocytosis at a CNS nerve terminal: faster kinetics at physiological temperatures and increased endocytotic capacity during maturation. J. Neurophysiol. *98*, 3349–3359.

Rosenmund, C., and Stevens, C.F. (1996). Definition of the readily releasable pool of vesicles at hippocampal synapses. Neuron *16*, 1197–1207.

Royle, S.J., and Lagnado, L. (2010). Clathrin-mediated endocytosis at the synaptic terminal: bridging the gap between physiology and molecules. Traffic *11*, 1489–1497.

Saheki, Y., and De Camilli, P. (2012). Synaptic vesicle endocytosis. Cold Spring Harb. Perspect. Biol. *4*, a005645.

Sankaranarayanan, S., and Ryan, T.A. (2001). Calcium accelerates endocytosis of vSNAREs at hippocampal synapses. Nat. Neurosci. *4*, 129–136.

Soykan, T., Kaempf, N., Sakaba, T., Vollweiter, D., Goerdeler, F., Puchkov, D., Kononenko, N.L., and Haucke, V. (2017). Synaptic Vesicle Endocytosis Occurs on Multiple Timescales and Is Mediated by Formin-Dependent Actin Assembly. Neuron *93*, 854–866.e854.

Sudhof, T.C. (2004). The synaptic vesicle cycle. Annu. Rev. Neurosci. *27*, 509–547.

Thévenaz, P., Ruttimann, U.E., and Unser, M. (1998). A pyramid approach to subpixel registration based on intensity. IEEE Trans. Image Process. *7*, 27–41.

Varoqueaux, F., Sigler, A., Rhee, J.S., Brose, N., Enk, C., Reim, K., and Rosenmund, C. (2002). Total arrest of spontaneous and evoked synaptic transmission but normal synaptogenesis in the absence of Munc13-mediated vesicle priming. Proc. Natl. Acad. Sci. USA *99*, 9037–9042.

von Gersdorff, H., and Matthews, G. (1994a). Dynamics of synaptic vesicle fusion and membrane retrieval in synaptic terminals. Nature *367*, 735–739.

von Gersdorff, H., and Matthews, G. (1994b). Inhibition of endocytosis by elevated internal calcium in a synaptic terminal. Nature *370*, 652–655.

Watanabe, S., Liu, Q., Davis, M.W., Hollopeter, G., Thomas, N., Jorgensen, N.B., and Jorgensen, E.M. (2013a). Ultrafast endocytosis at Caenorhabditis elegans neuromuscular junctions. eLife *2*, e00723.

Watanabe, S., Rost, B.R., Camacho-Pérez, M., Davis, M.W., Söhl-Kielczynski, B., Rosenmund, C., and Jorgensen, E.M. (2013b). Ultrafast endocytosis at mouse hippocampal synapses. Nature *504*, 242–247.

Watanabe, S., Trimbuch, T., Camacho-Pérez, M., Rost, B.R., Brokowski, B., Söhl-Kielczynski, B., Felies, A., Davis, M.W., Rosenmund, C., and Jorgensen, E.M. (2014). Clathrin regenerates synaptic vesicles from endosomes. Nature *515*, 228–233.

Watanabe, S., Mamer, L.E., Raychaudhuri, S., Luvsanjav, D., Eisen, J., Trimbuch, T., Sohl-Kielczynski, B., Fenske, P., Milosevic, I., Rosenmund, C., et al. (2018). Synaptojanin and Endophilin Mediate Neck Formation during Ultrafast Endocytosis. Neuron *98*, 1184–1197.e1186.

Wu, X.S., McNeil, B.D., Xu, J., Fan, J., Xue, L., Melicoff, E., Adachi, R., Bai, L., and Wu, L.G. (2009). Ca(2+) and calmodulin initiate all forms of endocytosis during depolarization at a nerve terminal. Nat. Neurosci. *12*, 1003–1010.

Wu, L.G., Hamid, E., Shin, W., and Chiang, H.C. (2014a). Exocytosis and endocytosis: modes, functions, and coupling mechanisms. Annu. Rev. Physiol. *76*, 301–331.

Wu, X.S., Zhang, Z., Zhao, W.D., Wang, D., Luo, F., and Wu, L.G. (2014b). Calcineurin is universally involved in vesicle endocytosis at neuronal and non-neuronal secretory cells. Cell Rep. *7*, 982–988.

Wu, Y., O'Toole, E.T., Girard, M., Ritter, B., Messa, M., Liu, X., McPherson, P.S., Ferguson, S.M., and De Camilli, P. (2014c). A dynamin 1-, dynamin 3- and clathrin-independent pathway of synaptic vesicle recycling mediated by bulk endocytosis. eLife *3*, e01621.

Yamashita, T., Eguchi, K., Saitoh, N., von Gersdorff, H., and Takahashi, T. (2010). Developmental shift to a mechanism of synaptic vesicle endocytosis requiring nanodomain Ca2+. Nat. Neurosci. *13*, 838–844.

Zhu, Y., Xu, J., and Heinemann, S.F. (2009). Synaptic vesicle exocytosis-endocytosis at central synapses: Fine-tuning at differential patterns of neuronal activity. Commun. Integr. Biol. *2*, 418–419.

STAR★METHODS

KEY RESOURCES TABLE

REAGENT or RESOURCE	SOURCE	IDENTIFIER
Bacterial and Virus strains		
Clathrin Knock Down f(U6)sNLS-RFPw-shRNA-mCHC#2	Charité Viral Core Facility	Cat#BL-0424
Clathrin Knock Down Scramble f(U6)sNLS-RFPw-Scr.shClathrin	Charité Viral Core Facility	Cat#BL-0360
Synaptophysin-pHluorin f(syn) CreOFF(Syphy)w	Charité Viral Core Facility	Cat#BL-0676
SynGCaMP6 f(syn)-CreOFF((Syp-GCamp6f))w	Charité Viral Core Facility	Cat#BL-1338
Chemicals, Peptides, and Recombinant Proteins		
APV	Tocris	Cat# 0106
Bicuculine methochloride	Tocris	Cat# 0131
NBQX disodium salt	Tocris	Cat# 1044
BAPTA-AM	Invitrogen	Cat# B6769
Dynasore	Tocris	Cat#2897
Latrunculin-A	Tocris	Cat# 3973
Tetrodotoxin citrate (TTX)	Tocris	Cat# 1069
Papain, suspension	CellSystems GmbH	Cat# LS003126
Ferritin cationized	Electron Microscopy Science (EMS)	Cat#15550
Experimental Models: Organisms/Strains		
Mouse: C57/BL6N (WT)	Charité Animal Facility	N/A
Mouse: Mun13-DKOs: Unc13atm1Bros; Unc13btm1Rmnd; background FVB/N	Augustin et al., 1999; Camacho et al., 2017; Varoqueaux et al., 2002	RRID: MGI:2654056
Software and Algorithms		
ImageJ	NIH	https://imagej.nih.gov
ImageJ StackReg Plug-in	Thévenaz et al., 1998	http://bigwww.epfl.ch/thevenaz/stackreg/
IMOD	University of Colorado	https://bio3d.colorado.edu/imod
Prism	GraphPad	https://www.graphpad.com/
Excel	Microsoft	https://www.office.com/
Axograph X	Axograph	https://axograph.com/
Other		
Sapphire disks, 6-mm	Wohlwend	Cat#1292
Leica EM-ICE	Leica Microsystems	https://www.leica-microsystems.com
Leica HPM100	Leica Microsystems	https://www.leica-microsystems.com
Leica AFS2	Leica Microsystems	https://www.leica-microsystems.com

LEAD CONTACT AND MATERIALS AVAILABILITY

Further information and requests for resources and reagents should be directed to and will be fulfilled by the Lead Contact, Melissa A. Herman (melissa.herman@charite.de). This study did not generate new unique reagents.

EXPERIMENTAL MODEL AND SUBJECT DETAILS

Primary neuronal cultures were generated from both sexes of postnatal mice from the C57/BL6N strain aged postnatal day 0-2 (P0-2) or embryonic mice from the Munc13-1/2 double knockout line at day 18 in embryonic development (E18). All experiments concerning

animals were performed to the regulations of the Animal Welfare Committee of the Charité Universitätsmedizin and the Berlin state government (permit # T0220/09).

Brains from wild-type (WT; C57/BL6N; P0-2) or Munc13-1/2 double knockout (Munc13DKO) or wild-type littermate (Munc13WT) animals (E18) were removed and placed in 4°C cooled Hank's Buffered Salt Solution (HBSS; GIBCO Life Technologies, Germany). Hippocampi were carefully dissected out and placed in Neurobasal-A Medium supplemented with B27, Glutamax, (all from GIBCO Life Technologies), and penicillin/streptavidin (Roche, Germany; full-NBA) at 37°C in a heated shaker. Full-NBA was replaced with Dulbecco's Modified Eagle Medium (DMEM; GIBCO), supplemented with 1 mM $CaCl_2$ and 0.5 mM EDTA (enzyme solution), containing papain (22.5 U/mL; CellSytems GmbH, Germany) and incubated for 45-60 min. The digestion was stopped by removing the enzyme solution and replacing it with an inactivating solution of DMEM supplemented with albumin (2.5 mg/mL) and tripsin-inhibitor (2.5 mg/mL; both Sigma-Aldrich). The inactivating solution was removed after 5 min, and replaced with full-NBA. Tissue was dissociated mechanically and cells were counted on a neubauer chamber. For fluorescence imaging experiments, dissociated hippocampal cells were plated on an astrocyte-layered glass coverslips at a density of approximately 100 cells/mm^2. For electron microscopy experiments, dissociated WT cell were plated on 6 mm carbon-coated sapphire disks (Wohlwend, Sennwald, Switzerland) at a density of approximately 250 cells/mm^2. Experiments were performed on neurons at DIV 13-18.

METHOD DETAILS

Cloning and molecular biology

Expression vectors for proteins or shRNA of interest were delivered to primary neurons by lentivirus. Cloning of expression vectors and preparation of lentiviral particles were performed by the Charité Viral Core Facility (Charité-Universitätsmedizin, Berlin). Lentiviral particles were prepared as previously described (Lois et al., 2002). Briefly, HEK293T cells were co-transfected the the lentivirus shuttle vector (10 μg) and two helper plasmids, pCMVdR8.9 and pVSV.G (5 μ g each) using polyethyleminine. After 72 hours, virus-containing supernatant was collected, filtered, aliquoted and flash-frozen with liquid nitrogen. Virus aliquots were stored at −80°C.

The synaptophysin-pHluorin (SypHy) vector, with the SypHy sequence flanked by LoxP sites, was previously cloned and described (Herman et al., 2018). For calcium imaging at the synaptic bouton, the genetically encoded calcium sensor, SynGCaMP6f (Chen et al., 2013; Grauel et al., 2016), was cloned into a LoxP site expression vector by the Charité Viral Core Facility (Charité Universitätsmedizin, Berlin). The complimentary DNA (cDNA) of either SypHy or SynGCaMP6f was cloned into the lentiviral expression vector, FUGW (Lois et al., 2002), containing LoxP sites. Expression of the probes was under the control of the human *synapsin-1* promoter. For clathrin knockdown experiments, shRNA again mouse clathrin heavy chain (5′-GTTGGTGACCGTTGTTATG-3′) or scrambled (5′-TTCGCACCCTACTTCGTGG-3′) shRNA sequences were previously cloned into FUGW (Lois et al., 2002) lentiviral vectors with U6 promoter driving shRNA expression (Watanabe et al., 2014).

Typically, lentivirus was added to primary neuronal cultures between 1-3 DIV. For clathrin knock-down experiments neurons were infected at 7 DIV with lentivirus expressing either scramble or clathrin heavy chain shRNA.

Live imaging of SypHy and SynGCaMP6f

Live imaging of SypHy and SynGCaMP6f was performed on an inverted microscope (Olympus IX51, Olympus, Tokyo, Japan). Samples were perfused with an extracellular solution containing the following (in mM): 140 NaCl, 2.4 KCl, 10 HEPES (Merck, NJ, USA), 10 glucose (Carl Roth, Karlsruhe, Germany), 2 $CaCl_2$, (Sigma-Aldrich, St. Louis, USA), 4 $MgCl_2$ (Carl Roth); 300 mOsm; pH 7.4. Field stimulation was achieved by passing current between platinum electrodes of a field stimulation chamber (Warner Instruments, CT, USA). NBQX (5 μM), bicuculine (15 μM), and AP-5 (10 μM) were included in all perfusion solutions. SynGCaMP6f experiments were performed at room temperature. SypHy experiments were performed at elevated temperature (~32-34°C) using simultaneously a custom-built in-line heating system and heated-collar for the objective (Warner Instruments).

Images were captured with a Hamamatsu ImagEM CCD camera under control of the Hamamatsu ImageLive software, using a 60X objective (1.2 n/a) and 2X2 binning. Samples were illuminated by light-emitted diode (LED; CoolLED, Andover, UK) at wavelength 470 nm for 100 ms at a capture rate of 1Hz (SypHy) or 5 Hz (SynGCaMP6f).

Electron microscopy

Primary hippocampal neurons grown on sapphire discs were transferred at 13-15 DIV to the chamber of a high pressure freezing machine (EM-ICE or HPM100, Leica, Wetzlar, Germany) and cryo-fixed in extracellular solution containing the following (in mM): 140 NaCl, 2.4 KCl, 10 HEPES (Merck), 10 glucose (Carl Roth), 2 $CaCl_2$, (Sigma-Aldrich), 4 $MgCl_2$ (Carl Roth); 300 mOsm; pH 7.4, or in the same extracellular solution with the addition of 250 mM sucrose. The concentration of 250 mM sucrose was chosen for EM experiments as it is high enough to cause substantial release, but still compatible with optimal sample processing after high pressure freezing. We found that 500 mM sucrose during freezing led to sub-optimal EM sample and image quality likely due to poor freeze-substitution and infiltration (data not shown). While 250 mM sucrose has been shown to release less of the readily-releasable pool during the transient component, the steady state current is roughly 80% of the steady-state current produced by application of 500 mM sucrose (Arancillo et al., 2013; Rosenmund and Stevens, 1996). All experiments were performed at 35°C unless otherwise stated.

To visualize endocytic structures neurons were incubated in a solution containing the fluid-phase marker ferritin prior to cryo-fixation as previously described (Watanabe et al., 2013b). Briefly, ferritin was included in the neuronal medium (full-NBA) at a concentration of 2.5 mg/mL for at least 5 min prior to cryo-fixation.

Cryo-fixation was followed by freeze-substitution in anhydrous acetone containing 1% glutaraldehyde, 1% osmium tetroxide and 1% milliQ water in an automated freeze-substitution device (AFS2, Leica). The temperature was kept for 5h at −90°C, brought to −20°C (5°C/h), kept for 12h at −20°C and then brought to +20°C (5°C/h). Once at room temperature, samples were en-bloc stained in 0.1% uranyl acetate in acetone, infiltrated in increasing concentration of Epoxy resin (Epon 812, EMS) in acetone and embedded in pure resin for 48h at 65°C. Sapphire discs were removed from the cured resin block by thermal shock. 50 nm thick sections were obtained using an Ultracut ultramicrotome (UCT, Leica) equipped with a diamond knife (Ultra 45, Diatome) and collected on formvar-coated 200-mesh or, for serial sections, formvar-coated slot copper grids (EMS). Sections were counterstained with uranyl acetate and lead citrate and imaged in a Tecnai G20 Transmission Electron Microscope (FEI) operated at 80-200 keV and equipped with a Veleta 2K x 2K CCD camera (Olympus).

QUANTIFICATION AND STATISTICAL ANALYSIS

Detailed statistical analysis can be found in Table S1. For all electron microscopy experiments, *n* represents the number of synaptic profiles imaged. For all live-imaging experiments, *n* represents the number of image sequences (fluorescence from identified areas of interest averaged over an entire field of view). Number of independent cultures per experiment are represented as *n/# of cultures*.

Live imaging of SypHy and SynGCaMP6f

Analysis of images was performed offline using ImageJ (National Institutes of Health), Axograph X (Axograph), and Prism 5 (GraphPad; San Diego, CA). For SypHy, image sequences were background-subtracted in ImageJ using the rolling-ball background subtraction (50 pixel) and aligned using a StackReg plug-in (Thévenaz et al., 1998) to correct for x-y drift when necessary. Regions of interest (ROIs) were selected from baseline-subtracted ammonium chloride application (50 mM). Values from image sequence ROIs measured in ImageJ were exported to Axograph and plotted at fluorescence (a.u.) per sequence frame. For SynGCaMP6f, ROIs for background or baseline-subtracted peak response to a 40 stimuli train at 20 Hz were selected from images sequences and plotted in Axograph as a.u. per sequence frame. Background ROIs were averaged, and the average background was subtracted from all measured ROIs. For all imaging experiments, ROIs were averaged per image sequence and the average value was treated as n = 1. Experiments were repeated in multiple independent cultures, with number indicated in figure legend per experiment as n = images/cultures. Statistical analysis of values measured from average images was performed in Prism. The statistical test used, as indicated in Table S1 or figure legends, was determined based on number of groups analyzed and the normality of the values' distribution (D'Agostino & Pearson normality test).

Electron microscopy

Image and analysis of EM micrographs was performed blind to experimental conditions. Identification of endocytic structures was performed manually in ImageJ. Counts of structures per synaptic profile were analyzed in GraphPad Prism. Significance was determined by pairwise Chi square tests of the number of profiles containing 0, 1, $\geq$ 2 structures of interest. As $\geq$ 2 structures happened rarely, this parameter was excluded if fewer than 5 observations were made. The total number of synaptic profiles analyzed for each condition is indicated in bar graphs (n) followed by the number of independent cultures. For quantification of endocytic pit localization relative to active zones, measurements were made in IMOD (University of Colorado, Boulder; http://bio3d.colorado.edu/imod/) from serially reconstructed synapses. Synaptic profiles with visible pits were targeted for serial reconstruction and data were collected from 13 reconstructed synapses.

DATA AND CODE AVAILABILITY

This study did not generate any unique datasets or code.

Cell Reports, Volume *29*

Supplemental Information

Calcium-Independent Exo-endocytosis Coupling at Small Central Synapses

Marta Orlando, Dietmar Schmitz, Christian Rosenmund, and Melissa A. Herman

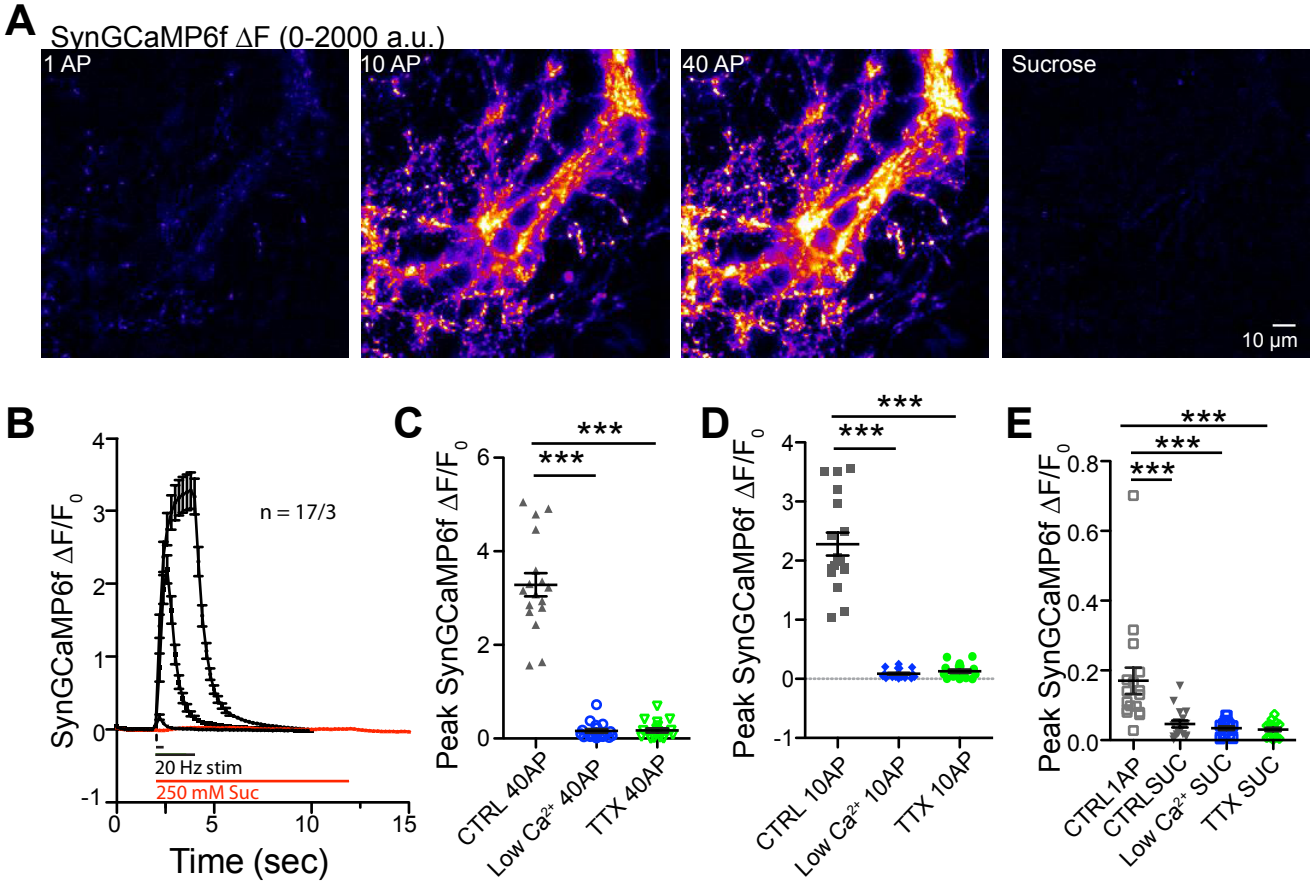

Figure S1. Sucrose application does not substantially activate SynGCaMP6f. Related to Figure 1. A) Peak fluorescence images of SynGCaMP6f in response to extracellular stimulation with 1 pulse to generate an action potential (AP), 10 pulses (20 Hz) or 40 pulses (20 Hz). B) Average SynGCaMP6f signals normalized to baseline fluorescence (F0) over time in response to indicated stimulation paradigms. C-D) Average peak SynGCaMP6f in response to 40 (C) or 10 (D) pulses under control conditions (gray) or in the presence of 0.1 mM $[Ca^{2+}]_e$ extracellular solution (Low Ca^{2+}; blue) or 1 μM TTX (green). E) Average SynGCaMP6f signal in response to 250 mM sucrose (10 s) made in control solution (gray), Low Ca^{2+} (blue), or 1 μM TTX (green). Sucrose signals in each condition were compared to the average single produced by a single pulse of electrical stimulation (gray open squares). All data are presented as mean ± sem. Significance for each set of data in panels C-E was determined by Kruskal-Wallis test with Dunn's Multiple Comparison post hoc test. ***$p \leq 0.001$

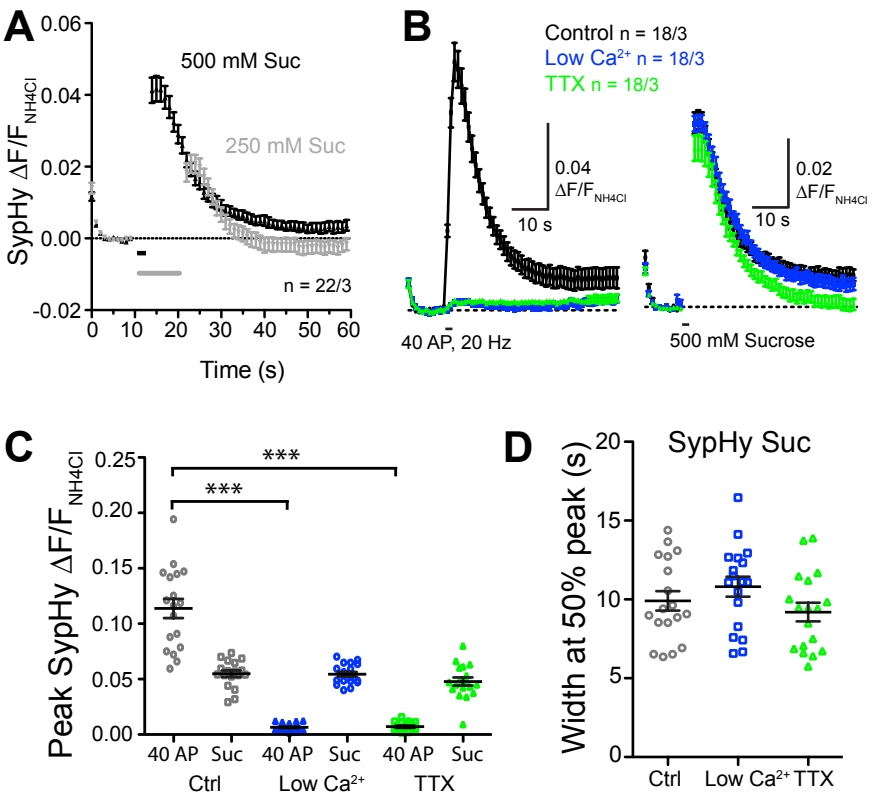

Figure S2. Sucrose evokes a robust SypHy response that is unaffected by $[Ca^{2+}]_e$ or TTX. Related to Figure 2. A) Average SypHy signal induced by application of 250 mM (10 s; gray) or 500 mM (2 s; black) sucrose normalized to the fluorescence response to ammonium chloride (NH_4Cl; 50 mM) over time. B) Average ammonium-normalized SypHy signal over time in control conditions, 0.1 mM $[Ca^{2+}]_e$, or TTX evoked by extracellular stimulation (40 pulses, 20 Hz) or sucrose (500 mM, 2 s). C) Comparison of peak ammonium-normalized SypHy responses from conditions represented in B. Significance determined by one-way ANOVA with Dunnett's multiple comparison post hoc test. ***$p \leq 0.001$ D) Comparison of the width of SypHy signals in response to sucrose at 50% of the peak in control (black), low Ca^{2+}, or TTX. Significance was determined by one-way ANOVA with Tukey'smultiple comparison post hoc test. Data in all panels are presented as mean ± sem.

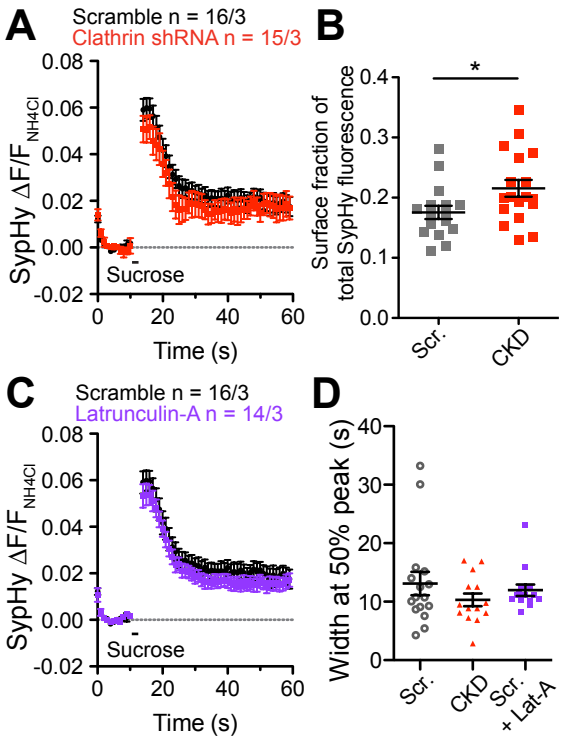

Figure S3. Decay of sucrose-evoked SypHy response is unaffected by clathrin knock down or inhibition of actin polymerization. Related to Figure 4. A) Average ammonium-normalized SypHy signal over time in response to 500 mM sucrose (2 s) in cultures expressing scramble shRNA (black) or clathrin heavy chain shRNA (red). B) Plot of total SypHy fluorescence fraction sensitive to application of a pH5.5 MES-buffered extracellular solution. *p = 0.035; unpaired t test. C) The same average SypHy signal from cultures expressing scramble shRNA as (A; black) compared to cultures expressing scramble shRNA with the addition of 5 µM latrunculin-A in the extracellular solution (purple). D) Average widths of ammonium-normalized SypHy signal at 50% of the peak in conditions described in (A) and (C). Data in all panels are presented as mean ± sem.

Figure	Condition	n	Cult.	Measurement	Mean	sem	Comparison	Test	p value	Comparison	Test	p value
1B	Control	252	3	Pits/profile	0.028	0.01	1B sucrose	Chi square	<0.0001			
1B	Sucrose	237	3	Pits/profile	0.2	0.031						
1D	Sucrose	13	1	Distance (nm)	95.6	11.8						
1G	Control Munc13 WT	319	4	Pits/profile	0.094	0.016	1G suc WT	Chi square	0.0001	1G control DKO	Chi square	0.004
1G	Sucrose Munc13 WT	150	4	Pits/profile	0.29	0.042	1G suc DKO	Chi square	<0.0001			
1G	Control Munc13 DKO	284	4	Pits/profile	0.028	0.01	1G suc DKO	Chi square	0.3325			
1G	Sucrose Munc13 DKO	369	4	Pits/profile	0.051	0.011						
2B	Field stim, sucrose	22	3	Fluorescence/time (s)								
2C	Field stim 20 Hz, 2s	22	3	Width at 50% peak (s)	9.24	0.36	2C field 10Hz	K-W; Dunn's	ns	2C sucrose	K-W; Dunn's	ns
2C	Field stim 10 Hz, 2s	22	3	Width at 50% peak (s)	8.57	0.27	2C sucrose	K-W; Dunn's	ns			
2C	500 mM sucrose, 2s	22	3	Width at 50% peak (s)								
2D	Control, dynasore	13	3	Fluorescence/time (s)								
2E	Control	13	3	% SypHy decay	13.42	3.21	2E dynasore	Paired t	<0.0001			
2E	Dynasore	13	3	% SypHy decay	84.01	11.48						
2G	Control	134	3	Pits/profile	0.06	0.021	2G sucrose	K-W; Dunn's	≤0.05			
		98	2	FT+ endosome/profile	0.051	0.034						
		98	2	FT+SVs/profile	0.01	0.01	2G 30s wash	K-W; Dunn's	≤0.05			
2G	Sucrose	165	3	Pits/profile	0.18	0.031						
		101	2	FT+ endosome/profile	0	0						
		101	2	FT+SVs/profile	0	0	2G 30s wash	K-W; Dunn's	≤0.01			
2G	10 s wash	164	3	Pits/profile	0.12	0.026						
		105	2	FT+ endosome/profile	0.038	0.019						
		105	2	FT+SVs/profile	0.086	0.033						
2G	30 s wash	143	2	Pits/profile	0.12	0.027						
		143	2	FT+ endosome/profile	0.077	0.024						
		143	2	FT+SVs/profile	0.23	0.076						
3B	Control	112	2	Pits/profile	0.11	0.032	3B sucrose	Chi square	0.0061	3B suc+BAPTA	Chi square	0.057
3B	Sucrose	149	2	Pits/profile	0.26	0.037	3B suc+BAPTA	Chi square	0.7871			
3B	Sucrose + BAPTA-AM	103	2	Pits/profile	0.22	0.043						
3D	0.1% DMSO	16	3	Peak SypHy F/F_{NH4Cl}	0.047	0.0016	3D BAPTA 5	Dunnett's	≤0.001	3D BAPTA 10	Dunnett's	≤0.001
3D	BAPTA-AM 5 min	13	3	Peak SypHy F/F_{NH4Cl}	0.032	0.0024						
3D	BAPTA-AM 10 min	9	2	Peak SypHy F/F_{NH4Cl}	0.028	0.0022						
3E	0.1% DMSO	16	3	Width at 50% peak	9.95	0.46	3E BAPTA 5	Dunnett's	≤0.01	3E BAPTA 10	Dunnett's	≤0.001
3E	BAPTA-AM 5 min	13	3	Width at 50% peak	12.66	0.65						
3E	BAPTA-AM 10 min	9	2	Width at 50% peak	14.87	0.75						
4B	Control, 25C	252	3	Pits/profile	0.028	0.01	4B suc, 25C	Chi square	0.0001			
4B	Sucrose, 25C	237	3	Pits/profile	0.202	0.031	4B suc, 35C	Chi square	0.9307			
4B	Control, 35C	198	5	Pits/profile	0.045	0.015	4B suc, 35C	Chi square	0.0002			
4B	Sucrose, 35C	216	5	Pits/profile	0.199	0.033						
4D	Control, scr. shRNA	131	2	Pits/profile	0.053	0.02	4D suc, scr.	Chi square	<0.0001	4D suc, CKD	Chi square	0.0218
4D	Sucrose, scr. shRNA	100	2	Pits/profile	0.31	0.05	4D suc, CKD	Chi square	0.1558			
4D	Sucrose, Clathrin KD	108	2	Pits/profile	0.23	0.049						
4F	Control	184	3	Pits/profile	0.05	0.016	4F sucrose	Chi square	<0.0001	4F suc + lat-A	Chi square	0.7182
4F	Sucrose	151	3	Pits/profile	0.26	0.038	4F suc + lat-A	Chi square	0.0003			
4F	Sucrose + latrunculin A	158	3	Pits/profile	0.07	0.02						

Kruskal-Wallis (K-W), Dunn's Multiple Comparison Test

One-way analaysis of variance, Dunnett's Multiple Comparison test

n = synaptic profiles (EM experiments) or image sequences (live-imaging experiments)

Table S1. Quantification and statistics related to STAR methods for data presented in Figures 1-4.